J. Min. Metall. Sect. B-Metall. 54 (2) B (2018) 233 - 241

Journal of Mining and Metallurgy, Section B: Metallurgy

FORMATION MECHANISM OF Fe-Mo MASTER ALLOY BY ALUMINOTHERMIC REDUCTION OF MoS_2-Fe_2O_3 IN THE PRESENCE OF LIME

M.H. Golmakani, J. Vahdati khaki*, A. Babakhani

Department of Metallurgical Engineering, Faculty of Engineering, Ferdowsi University of Mashhad, Mashhad, Iran

(Received 16 March 2018; accepted 23 June 2018)

Abstract

The reaction mechanism of MoS_2-Fe_2O_3 aluminothermic reduction in the presence of lime using microwave-assisted combustion synthesis method was surveyed. Achieving technical feasibility in one-step production of ferromolybdenum along with sulfur removing in solid form are the main features of this novel process. Simultaneous Preliminary thermo-analytical investigations DSC/TGA and X-ray diffraction experiments during the heating process of $0.42MoS_2 + 1.14Al + 0.29Fe_2O_3 + 0.84CaO$ demonstrated four key sequential endothermic and exothermic reactions at 420, 540, 660, and 810°C. The most noteworthy reactions involve evaporation of moisture and volatile matter, molybdenite roasting, simultaneous production of lateral compounds such as $CaMoO_4$ and $CaSO_4$, aluminum melting transition, and final termite reaction. Kinetics procedure of the system was conducted using a classical model-free approach by Kissinger–Akahira–Sunose (KAS) method. In this study, the activation energy was determined about 106.4 ($kJ.mol^{-1}$) for thermite reaction in the temperature range of 810 to 918°C.

Keywords: *Aluminothermic reduction; Thermo-analytical; Ferromolybdenum; Kinetics; Activation energy*

1. Introduction

One of the most common methods for Ferromolybdenum production is implementing Pyro-metallurgical process on molybdenum sulfide concentrate, which involves two separate phases: 1-oxidative roasting of molybdenite (MoS_2) in the temperature range of 500-650°C, and 2-metallothermic reduction of produced molybdenum trioxide in the presence of iron oxides, with or without ferrous scrap as diluent material [1-5]. Apart from the considerable molybdenum loss caused by the evaporation of molybdenum compounds in the oxidative roasting stage, other problems could also arise as a result of using aluminothermic reduction process including environmental pollution caused by emissions of sulfur gases, costly separation processes, and also the demand for excessive time and energy due to two-step process of ferromolybdenum manufacturing [6-7]. Mehra and Gupta conducted the first preliminary studies on the production of Ferromolybdenum from the molybdenite by aluminothermic reaction in the presence of calcium molybdate as sulfur adsorbent [8]. Mankhand et al., also conducted studies on the removal of molybdenite sulfur in the presence of lime [9]. Lillvier examined the carbothermic reaction of molybdenite in the presence of sodium carbonate by thermal dissociation in plasma arc furnace [10]. Parasad et al., have also investigated the feasibility reaction of sulfur removal by lime in MoS_2 and further studies were carried out on the removal of sulfur using limestone and carbon in plasma arc furnaces [11-12]. Suri, also used calcium hydroxide as a sulfur absorber to produce calcium molybdate from molybdenite [13]. In a similar study Afsahi et al., also found that molybdenum disulphide in the presence of lime and water can lead to the production of calcium molybdate along with a calcium sulfide solid phase [14]. Thermodynamic evaluations and preliminary experimental results in present study show that the direct production of ferromolybdenum from the molybdenum sulfide concentrate in the presence of lime as desulfurization agent could be possible in one step using aluminothermic reduction method [15]. Thus, the roasting of molybdenite and its molybdenum loss could be obviated to a considerable extent. Apart from saving time, cost and also energy, environmental problems caused by the emission of gaseous sulfur compounds in the roasting process could also be addressed since significant amounts of sulfur is crystallized in the form of solid calcium sulfide (CaS) as one of the slag phases of combustion synthesis reaction.

**Corresponding author:vahdati@um.ac.ir*

DOI:10.2298/JMMB180316011G

In this study, after a preliminary statement of problem and an overview of reaction conditions, kinetics of performed reactions and the sequence of these reactions will be discussed based on DSC-TGA thermal analysis method.

Certainly, there is not much to be investigated regarding the mechanism and kinetics of ferromolybdenum master alloy production especially by combustion synthesis process. However, significant studies have been done with regard to the kinetics of molybdenum compounds, especially molybdenite roasting and molybdenum oxide reduction processes. For example, Munz and Gauvin studied the kinetics of molybdenite decomposition in argon plasma [16]. Nita et al., have also covered the self-diffusion phenomenon in Fe-Mo systems [17]. Thermite reaction kinetics of the alumina and molybdenum trioxide in the production of Al-MoO_3 nanocomposites have also investigated by Schoenitz et al., [18]. Kim et al., carried out extensive studies on the kinetics of molybdenum compounds, including the study of the reduction kinetics of molybdenum oxide by hydrogen, and also kinetics investigations of oxidative roasting of molybdenite concentrate under optimal conditions for the production of molybdenum trioxide [19,20]. They also conducted studies on ferromolybdenum production through a two-step hydrogen reduction method [21]. Gan et al., have also studied the reaction mechanism of molybdenite during calcification roasting process [22].

With regards to the aforementioned issues, various combustion synthesis reactions were carried out with varying percentages of molybdenum in produced ferromolybdenum. Selection of the desired composition was done based on iron-molybdenum binary phase diagram, and also the compliance of the produced ferromolybdenum with available commercial standards [1-3].

Accordingly, the proposed response was expressed as a reaction (1):

$$0.42MoS_2 + 1.14Al + 0.29Fe_2O_3 + 0.84CaO = 0.42Mo - 0.56Fe + 0.57Al_2O_3 + 0.84CaS \quad (1)$$

Following this reaction, the produced ferromolybdenum will contain molybdenum mole fraction (42%), equivalent to 55 wt% Mo which as well as meeting the range of molybdenum percentages in commercial ferromolybdenum used in industry. It will also have the minimum requirements for product manufacturing from the point of view of adiabatic reaction temperature, slag fluidity, metal-slag interaction and also acceptable efficiency of produced molten ferromolybdenum droplets taken from raw materials under the combustion synthesis process.

Measuring the adiabatic temperature of reaction 1, according to Merzhanov's empirical criterion in Eq. 2, will show that the adiabatic temperature of this reaction with 55wt % Mo reaches to 2613K which is much higher than the Merzhanov's acceptance criterion (T_{ad} > 1800K) and therefore it can be classified in the range of self-propagation high temperature synthesis reactions (SHS)[15,23-24].

$$-\Delta H^{O}_{298} = \int_{298}^{T_{tr}} nC_p^{product}\,dT + n\Delta H_{tr} + \int_{T_{tr}}^{T_{ad}} nC_p^{product}\,dT \quad (2)$$

2. Material and method

In this study, high purity raw materials powders including aluminum (Rankem A2265; +99%, -45µm), iron oxide (Merck 103924; +99%, -45 µm), lime (Merck 102109; +97%, -25 µm) and molybdenum sulfide (Merck 11225; +98%, -25µm) were used. The raw materials were weighed according to the stoichiometric ratios in Eq. 1 and then were mixed in a ceramic mortar. The powder mixture was poured into a cylindrical mold, 20 mm in diameter, and was compressed at a pressure of 2-3MPa within five-minute dwell time in a hydraulic press. Compressed samples were placed in a microwave under air atmosphere. After approximately short period of time of about 5 to 20 seconds, the combustion synthesis reaction started from a tiny point at the surface of the sample and then the combustion front developed quickly across the volume of sample in a fraction of time (1-2 seconds).

To investigate the kinetics and sequence of the reactions, DSC-TGA thermal analyzer (Cetaram; SETSYS Evolution–1750) device was utilized which is capable of performing differential scanning calorimetry and thermogravimetic analysis simultaneously at a temperature range of 25-1100°C in air environment and at heating rates of 5-20K/min.

Having analyzed the DSC graph and finding the temperature positions of the endothermic and exothermic peaks, other series of compressed bulk samples were placed in a laboratory induction furnace at a heating rate of 5K/min. Then the specimens were removed from the furnace at the same temperature peaks which were already observed in DSC graph, and then they were analyzed by X-rays diffraction analysis.

To identify the probable products of the reactions, X-Ray diffraction analysis (XRD: Philips Analytical X-Ray B.V_Cu kα radiation) was used. Respective microstructures were also investigated by scanning electron microscopy (SEM: Leo 1450vp)

3. Results & discussion

3.1. Phase analysis

After combustion synthesis of the bulk sample in microwave in atmospheric pressure, the synthesized

ferromolybdenum droplets were analyzed by X-ray diffraction analysis. Meanwhile, these droplets were subjected to scanning electron microscopy (SEM), and chemical microanalysis technique through Energy Dispersive X-ray Spectrometry (EDS).

In Fig. 1(a), the results of the XRD analysis show the presence of Fe_3Mo_3C and Fe_3Mo phases. Besides, the semi-quantitative analysis of the two main phases using Reference Intensity Ratio (RIR) method shows that the proportions of Fe_3Mo_3C phase is equal to 65-70% and Fe_3Mo phase is equal to 30-35%. Also for elemental analysis of these compounds, mass fraction calculations can easily be done.

In Fig. 1(b), the semi–quantitative elemental analysis of two dominant phases is given in a table particularly for iron and molybdenum elements. It should be noted that the data in EDS analysis are normalized. Accordingly, phases 1 and 2 in the SEM image could probably be equivalent to the Fe_3Mo_3C and Fe_3Mo phases, respectively.

In Fig. 1(c), the approximate percentages of phases in the SEM image were obtained by means of Metallographic Image Processing (MIP) software. These results are relatively in accordance with the results in Fig 1(a) obtained by the RIR method.

It can be observed that in the previous investigation carried out by the present authors, the combustion synthesis of the sample in the argon inert atmosphere was also studied, and in terms of reaction products, the results were almost the same [15]. It can be deduced that in the process of combustion synthesis performed in this study, the atmosphere of the environment, due to the very short time of the SHS process, has no significant effect on the type and composition of the products.

The point to be considered is that by applying the RIR Method in the X-ray diffraction pattern in Fig. 1(a), Fe_3Mo_3C carbide phase (incl. a stoichiometric carbon percentage of 2.5 wt %), has been observed as the dominant phase.

However, carbon percentage of phase 1 measured by the EDS analysis in Fig. 1(b) is very low and the applied laboratory raw materials in reaction 1 are of high purity too. Therefore, it seems that Fe_3Mo_3C phase in the X-ray diffraction analysis could be assumed as a non-stoichiometric compound, $Fe_3Mo_3C_{1-x}$. Regarding this isuue, sufficient explanation can be found in other articles by the present authors and also Di et al, [15, 25]. Therefore, based on the above-mentioned argument, this phase can be assumed to be equivalent to the Sigma phase (σ-FeMo) in Fe-Mo phase diagram [2, 26-27].

3.2. Formation mechanism

DSC-TGA thermal analyses were used to investigate the kinetics and sequence of chemical reactions in relation to reaction 1. To provide a more accurate identification of the peaks obtained from the thermal analysis, the DSC results of two main raw materials including MoS_2 and CaO are shown in Fig 2. In the DSC analysis of all samples, the 5K/min heating rate and the air atmosphere were selected. In Fig. 2(a) an exothermic peak is observed in 514ºC that can be related to the oxidative roasting of molybdenite. In Fig. 2(b) two endothermic peaks are visible at the temperatures of 433ºC and 674ºC. Other studies show that the first peak is associated with the decomposition of $Ca(OH)_2$ and the second peak pertains to the calcination of minor calcium carbonate in CaO raw material [28-30].

It should be noted that phases $Ca(OH)_2$ and $CaCO_3$ are also observed in the XRD graph prepared from the lime raw material.

A bulk sample containing all the components in Reaction 1, according to the stoichiometric ratio, was prepared exactly in the same way as samples used in the combustion synthesis process and subjected to DSC-TGA analysis. Since this sample can eventually lead to the production of ferromolybdenum master alloy, the abbreviation $FeMo_{Mix}$ is adopted in this study. Also, two other bulk samples comprising dual compounds of $0.29Fe_2O_3$-1.14Al and $0.84CaO$-$0.42MoS_2$ were subjected to the DSC-TGA thermal analysis. In Fig. 3, the DSC graphs are shown for these three samples. As it is shown, a very good match in the temperature range of the endothermic peaks of 422-426°C can be seen in the two $FeMo_{Mix}$ and CaO-

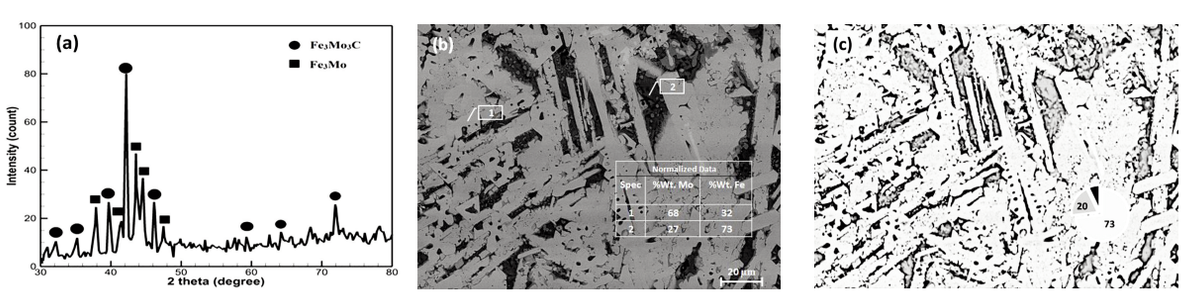

***Figure 1**. Analysis results of synthesized ferromolybdenum droplets in microwave, (a) X-Ray diffraction pattern, (b) SEM micrograph along with the EDS analysis of two dominant phases, (c) image processing of existence phases in image (b)*

MoS_2 samples. Of course, this peak is also observed in Fig. 2(b).

At 520-550ºC, the same agreement is also found between exothermic peaks of two $FeMo_{Mix}$ and CaO-MoS_2 graphs. This peak is also visible in Fig. 2(a).

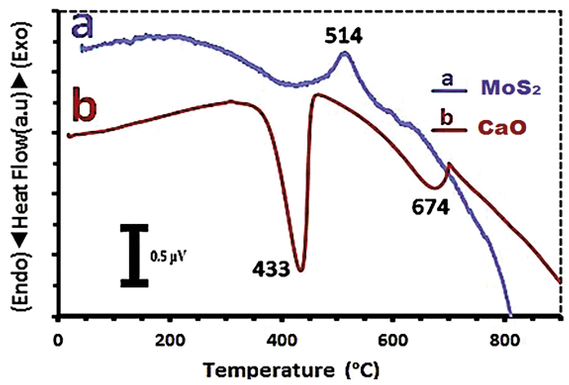

***Figure 2**. DSC thermo-analytical curves at 5K/min heating rate under air atmosphere for, (a) MoS_2, (b) CaO*

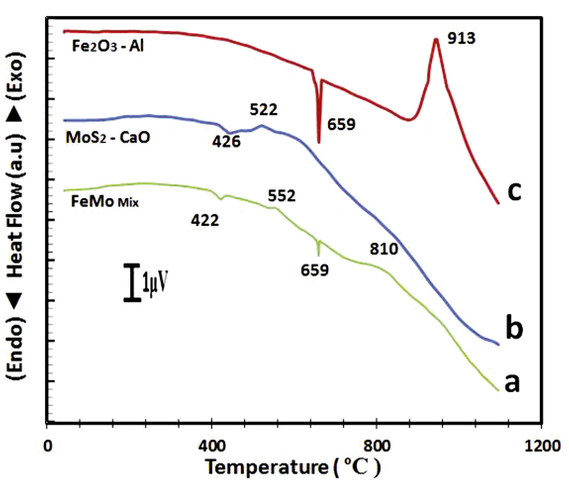

***Figure 3**. DSC thermo-analytical graphs at heating rate of 5K/min under air flow for, (a) $FeMo_{Mix}$ Incl. Al-Fe_2O_3-MoS_2-CaO, (b) MoS_2-CaO, (c) Fe_2O_3-Al*

The peak of the aluminum melting transformation is also found at 659°C in the samples containing aluminum powder. To identify the sequence of probable reactions in the $FeMo_{Mix}$ sample, a thorough description of each existing peaks in the $FeMo_{Mix}$ graph will be discussed in the following.

Hence, in Fig. 4, for the sake of more clarity, the DSC graph of the $FeMo_{Mix}$ powder mixture with its thermogravimetric curve at 5K/min heating rate is plotted again. To provide a more comprehensive and in-depth interpretations of thermal analysis results, Derivative Thermogravimetric Analysis (DTGA) curve is plotted in Fig. 4(c) to specify the inflection points.

3.2.1. Endothermic peak at 422ºC

First, it is necessary to explain that in the range of 100-120ºC, the results of the DSC thermal analysis in Fig. 4(a), apart from a partial detachment, do not show any sign of the thermal peak. However, weight loss with a fairly significant slope in Fig. 4(b) indicates a physical transformation in this temperature range. Also, this inflection point as a well-defined peak is clearly observed in DTGA curve in Fig. 4(c). This peak seems to be formed due to the removal of the initial moisture content found in the raw materials.

The first indicator peak in Fig. 4(a) is attributed to the endothermic peak, which initiates at 406ºC and reaches its maximum at 422ºC.

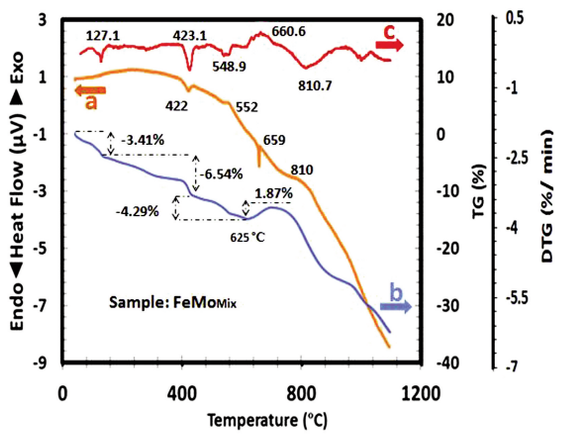

***Figure 4**. Simultaneous thermal analysis results of $FeMo_{Mix}$ at 5K/min heating rate under air atmosphere, (a) DSC Curve, (b) Thermogravimetric graph,(c) DTGA Curve*

It seems that the presence of this endothermic peak arises due to the release of volatile matters and moisture content especially in lime/slaked lime and molybdenum sulfide raw materials. It should be noted that in the similar research carried out by Gan et al., the reason for the presence of these endothermic peaks in this temperature range was attributed to the release of moisture and volatile matters [22]. Also in Fig. 2(b), the presence of a peak at 433ºC could be caused by the dehydration of $Ca(OH)_2$ [28-29].

In Fig. 3(b), DSC graph of the MoS_2-CaO dual mixture, an endothermic peak similar to endothermic peak in Fig.4 (a) is visible at the temperature range of 400-450ºC too. To provide a plausible comparison of the thermogravimetric results and proof of the similarities of these endothermic peaks in these two powder mixture (i.e. $FeMo_{Mix}$ and CaO-MoS_2), the DSC-TGA curves of MoS_2-CaO mixture are shown in Fig. 5. The good match between these two peaks in Figs. 4 and 5, in terms of temperature, approximate proportional weight loss and also very similar descending slopes in the thermogravimetric analysis

of these two samples in temperature range of 25-450ºC, can enhance the possibility of the identical nature of these two peaks.

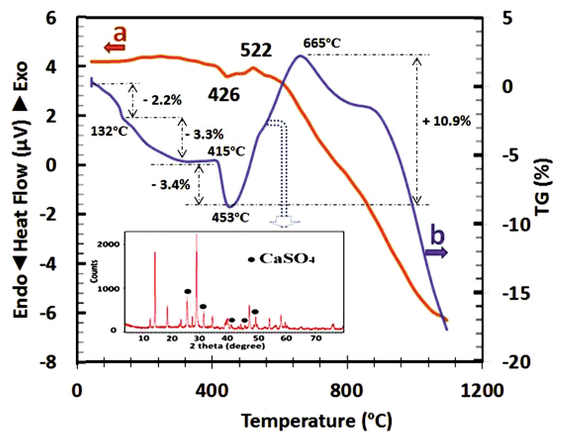

Figure 5. DSC-TGA curves of MoS_2-CaO mixture at 5K/min heating rate in atmospheric pressure (a) DSC graph, (b) TGA graph, which contains the XRD analysis of sample at 600ºC

In Fig. 6(a), the results of the X-ray diffraction analysis at 400ºC also show the absence of any new produced phase other than the reactants involved in reaction 1. It seems that the absence of a new phase in XRD results can confirm the theory of the outflow of moisture and volatile substances in this temperature range. It should be noted that in order to perform X-ray diffraction analysis, samples of powder mixture, similar to DSC samples, were placed in a laboratory induction furnace under atmosphere pressure and were heated at the rate of 5K/min from ambient temperature to the temperatures of index peaks that are shown in the DSC thermal analysis spectrum. The samples are then removed from the furnace and subjected to X-ray diffraction analysis.

Regarding Figs. 6(a) and 6(b) and the presence of the $Ca(OH)_2$ phase in the XRD analysis results, it can be stated that after the sample was removed from the furnace, there was a possibility of re-absorption of moisture by lime [29]. In fact, calcium oxide raw material, after the heating operation in the furnace, received moisture during cooling process and was converted into calcium hydroxide.

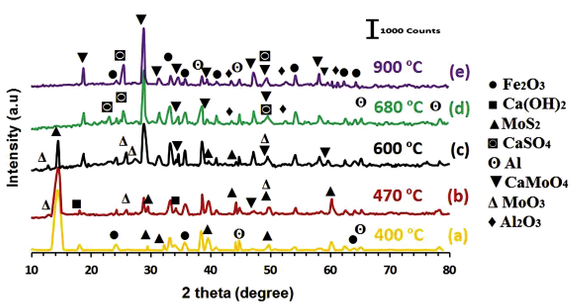

Figure 6. X-ray diffraction analysis results of the $FeMo_{Mix}$ specimen at different temperature (a) 400ºC (b) 470ºC, (c) 600ºC, (d) 680ºC, (e) 900ºC

3.2.2. Exothermic peak at 552ºC

In Fig. 4(a), a fairly small exothermic peak is visible in the range of 530-560ºC. This peak is clearly distinguishable in DTGA curve in Fig. 4(c).

With regards to molybdenite roasting temperature range, it seems that the main factor in the formation of this exothermic peak could be MoS_2 partial oxidative roasting phenomenon.

In Figs. 2(a), 3(a), and 3(b), the presence of this exothermic peak in DSC curves is seen. However, in Fig.3(c), it is not observed. Therefore, the simplest explanation for this result could be that the presence of this peak is dependent on MoS_2 and CaO compounds. In fact, the presence of this exothermic peak in DSC results in the first step can be explained by the following reaction [20]:

$$MoS_2 + 3.5O_2 = MoO_3 + 2SO_2 + Q \quad (3)$$

This exothermic reaction is accompanied by noticeable stoichiometric weight loss (10%) in the case of full roasting process of molybdenum sulfide to molybdenum trioxide. However, the presence of MoS_2 phase in significant amounts at 600°C in Fig.6(c) completely eliminates the possibility of fully performing this reaction. The presence of powder compounds such as lime, aluminum and iron oxide seems to somewhat prevent the reaction of molybdenite with oxygen by providing a protective barrier film and play the role of an inhibitor coating.

In the next step, formation of $CaMoO_4$ compound as another exothermic reaction could also be considered in accordance with reaction 4 [22]:

$$CaO + MoO_3 = CaMoO_4 + Q \quad (4)$$

Meanwhile, the results of the XRD analysis at around the temperature of this peak (Figs. 6(b) and 6(c)) indicate that the $CaMoO_4$ phase is also formed in small quantities. In fact, after molybdenite roasting and production of MoO_3, some of the molybdenum trioxide is evaporated due to its high vapor pressure, especially at temperatures close to 550-650°C. While, if the conditions for the formation of $CaMoO_4$ had been achieved, it would have inevitably prevented from evaporation of MoO_3 to a large extent [31].

In addition, according to the available references and thermodynamic calculations, the probability of the presence of the $CaSO_4$ phase in this temperature range should not be ignored with respect to the following reactions [22]:

$$2CaO + MoS_2 + 0.5O_2 = 2CaS + MoO_3 + Q \quad (5)$$

$$2CaS + 4O_2 = 2CaSO_4 + Q \quad (6)$$

And the main reaction (7) is obtained from the combination of these two reactions (5) and (6):

$$2CaO + MoS_2 + 4.5O_2 = 2CaSO_4 + MoO_3 + Q \quad (7)$$

Reaction (7) can also be derived from the integration of chemical reaction (3) with the following equation.

$$2CaO + SO_2 + O_2 = 2CaSO_4 + Q \quad (8)$$

The point to be considered is that if the process is carried out in accordance with each of these reactions (5-8), the weight gain of the specimen will be observed. Though, the weight loss of the $FeMo_{Mix}$ sample at 450-625°C (near to melting point of aluminum) is estimated to be about 4% in TGA curve in Fig. 4(b), which is in contrast with the weight gain in reactions (5-8).

The results of the X-ray diffraction analysis of $FeMo_{Mix}$ sample in the range of 450-620°C, (Figs. 6(b) and 6(c)) also show that $CaSO_4$ phase is not formed in this range. The lack of the $CaSO_4$ phase seems to be due to the relatively low weight percentages of MoS_2 and CaO components (Sum: 59 wt %) in comparison with the total weight of $FeMo_{Mix}$ sample.

While, in the XRD pattern shown in Fig. 5, in the case of MoS_2-CaO mixture without the presence of Al and Fe_2O_3, the presence of $CaSO_4$ phase in the similar temperature range (i.e., 450-620°C) is quite evident.

Moreover, in Fig.5 (b), the thermogravimetric analysis of the binary mixtures of CaO-MoS_2, in the range of 450-660°C is displayed; and the weight gain is also observed in contrast to the $FeMo_{Mix}$ sample which can be assumed as a direct result of the production of the $CaSO_4$ phase according to the above-mentioned reactions in CaO-MoS_2 mixture.

So, in order to sum up the main reasons for weight loss in the temperature range of 450-620°C in Fig. 4(b), the basic points include: a little SO_2 egression due to partial oxidation of MoS_2, partial evaporation of MoO_3, and impossibility of forming the $CaSO_4$ phase. It seems that the key reason for all of these points is the lack of complete reaction of molybdenite with lime. In fact, due to the presence of Al and Fe_2O_3 accompanied by CaO and MoS_2 in the $FeMo_{Mix}$ powder mixture, the possibility of forming a calcium sulfate phase ($CaSO_4$) cannot be obtained kinetically, and as a result, the weight gain along the formation of this phase, according to relations (5,6), will not occur.

3.2.3. Endothermic peak at 660°C

Certainly, this peak pertains to the endothermic melting reaction of the aluminum powder in the $FeMo_{Mix}$ mixture, which is visible in Fig. 3(a). In addition, this peak is also visible in the Al+Fe_2O_3 mixture graph in Fig. 3(c). Liu et al., provided a complete report on the DSC curve of Al+Fe_2O_3 mixture, as well as the conditions for the formation of various combinations of these two compounds [32].

What is noteworthy about this peak in Fig.3 (a-c) is that the enthalpy amount of the aluminum melting transformation in curve (a) is lesser than the one in curve (c).

The enthalpy value of the aluminum melting reaction in $FeMo_{Mix}$ sample is 4.32 µV.s/mg, while this amount is 16.19 µV.s/mg in the Al-Fe_2O_3 powder sample.

Considering that the weight of 1.14Al-0.29Fe_2O_3 sample covers 41% of the total $FeMo_{Mix}$ mixture weight (consisting of 4 components as raw materials in eq. 1), it can be concluded that the heat of the melting reaction of aluminum in $FeMo_{Mix}$ sample should be about 41% of the enthalpy amount of aluminum melting transition in Al-Fe_2O_3 sample, i.e. 6.64 µV.s/mg.

However, practically the value showed in the $FeMo_{Mix}$ graph (i.e.4.32µV.s/mg) is also slightly lower than this calculated value.

This difference can be due to the partial reactions between aluminum and lime, and in particular molybdenum disulfide. In fact, these partial reactions result in the consumption of some of the aluminum present in the sample. Of course, it should be noted that due to the small quantities of these reactions, there are no possibility of observing the proportional compounds of Al-Mo [33] or even Al-Ca-Mo-S components in the XRD graph.

In Fig. 6(d), the results of the XRD analysis in this temperature range show the complete removal of the MoS_2 and MoO_3 peaks and also increase in intensity of $CaMoO_4$ and $CaSO_4$ phases peaks.

3.2.4. Exothermic peak at 810°C

In fact, this peak could be introduced as the thermite reaction peak. The ignition temperature is 730°C and it reaches its maximum in combustion temperature of 810°C. The clear presence of this peak is also confirmed at DTGA curve in Fig. 4(c). This exothermic reaction is accompanied by a significant decrease in weight, which might be caused due to the noticeable decomposition of the $CaSO_4$ phase and the production of calcium sulfide (CaS) in this temperature range after the combustion synthesis reaction.

Though, the XRD analysis of $FeMo_{Mix}$ powder mixtures in this temperature range (Fig.6(e)), does not show these results. It seems that the reason for this issue can be spotted in the fundamental differences between the specimen conditions during the DSC-

TGA analysis and what is performed on specimen maintenance in induction furnace for providing the XRD samples.

Undoubtedly, the maintenance conditions in the induction furnace cannot be controlled compared to the DSC thermal analysis device.

It seems that the conditions of sample placement and maintenance from the ambient temperature in the laboratory furnace with different oxidation rate in this atmosphere have caused more oxidation of aluminum at lower temperature (Fig. 6(d)) and prevent the combustion synthesis reaction in next step, contrary to what is done in the DSC-TGA thermal analysis device.

It should be noted that, in spite of frequent samplings in the induction furnace at the temperature ranges between 800–900°C, contrary to our expectation, the combustion synthesis reaction in a furnace was not observed, and, in fact, the sintered specimens without the expected combustion synthesis reaction were subjected to X-ray diffraction analysis.

For this reason, in Fig. 6(e), in the XRD pattern at 900°C, the phases $CaMoO_4$, Fe_2O_3, $CaSO_4$ and even Al_2O_3 are also observed. The presence of aluminum and aluminum oxide phases without creating the thermite reaction shows that aluminum was not able to fulfill its mission to carry out combustion synthesis reaction and had practically not acted as a reduction agent.

Meanwhile, the weight increasing due to the presence of $CaSO_4$ and Al_2O_3 phases and the lack of decomposition of calcium sulfate at 900°C, in accordance with Fig. 6(e), practically makes it impossible to justify the weight reduction at this temperature range in the Thermogravimetric curve in Fig. 4(b).

It should be noted that the decomposition of $CaSO_4$ phase is highly dependent on the temperature and partial pressure of O_2 and SO_2. For example, in the atmospheric air (PO_2= 0.21) and very low partial pressure of SO_2 it begins in the temperature range of 800-900°C, and with increasing the SO_2 partial pressure shifts to higher temperatures value [22, 34].

Therefore, in order to observe the combustion synthesis process in furnace, the $FeMo_{Mix}$ sample, instead of gradual heating from ambient temperature (25ºC) to the synthesis reaction temperature, was placed inside the furnace at the initial temperature of 750ºC; and heating process for the specimen started from this temperature with rate of 5K/min, until the occurrence of the combustion synthesis phenomenon. Using this technique, SHS phenomenon occurred at 850°C, which is consistent with the temperature of exothermic peak in $FeMo_{Mix}$ specimen in Figs. 3(a) or 4(a). After the synthesis process, the ferromolybdenum droplets were separated from slag matrix, and the slag was subjected to XRD analysis.

In Fig. 7, XRD analysis of slag phase is displayed separately. As it is shown, the produced slag contains the main CaS, Al_2O_3 and $CaMoO_4$ phases, and also the calcium-dialuminate phase ($CaAl_4O_7$) at low value. The conditions for the formation of iron-sulfur compounds, especially iron sulfides, are also reasonable [35]. The presence of the CaS phase among the slag components demonstrates the probability that the $CaSO_4$ phase produced in the previous stages at lower temperatures of heating process, would be completely decomposed due to high temperature of combustion synthesis reaction and this argument could be viewed as a reason for weight loss in TGA curve of the $FeMo_{Mix}$ sample during and after the combustion synthesis, as shown in Fig. 4(b).

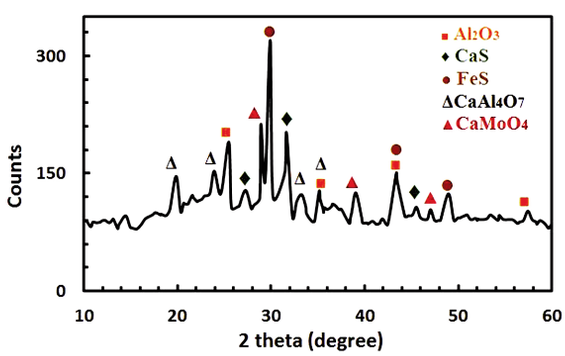

Figure 7*. XRD analysis of slag phase after realization of combustion synthesis phenomenon*

3.3. Kinetics procedure

Model free isoconversional kinetic analysis of DSC thermo-analytical data has been used to determine apparent activation energy in this system. In order to study the activation energy of the combustion synthesis reaction of the $FeMo_{Mix}$ powder mixture consisting raw materials of the reaction 1, the DSC thermal analysis of the samples was performed at three heating rates of 5,10, and 20K/min and monitored under air atmosphere and non-isothermal conditions from 25 to 1100ºC.

In Fig. 8, the results of the DSC thermal analysis from the $FeMo_{Mix}$ specimen are displayed at different heating rates in the air atmosphere. In order to determine the apparent activation energy of thermite reaction, the Kissinger-Akahira-Sunose (KAS) model was used [36-39].

Basic kinetics relation under non-isothermal conditions is described by the following equation for the degree of reaction α.

$$\frac{d\alpha}{dt} = \frac{A(\alpha)}{\beta_i} exp\left(\frac{-E(\alpha)}{RT}\right) f(\alpha) \qquad (9)$$

Where E (α) is the apparent activation energy (kJ.mole^{-1}) depending on the extent of reaction α, A(α) is the pre-exponential factor (s^{-1}) and f (α) is expressed the conversion factor reflecting the mechanism of the reaction, and with constant heating rate of $\beta_i = dT/dt$.

Solving the temperature integral of Eq. (9) using several approximations lead to one of the most popular iso-conventional method by Kissinger-Akahira-Sunose (KAS) model.

$$\frac{d\alpha}{dt} = \frac{A(\alpha)}{\beta_i} exp\left(\frac{-E(\alpha)}{RT}\right) f(\alpha) \qquad (10)$$

Where C_k (α) is equal to ln (AR/E_α).

Table 1. *The required information according to KAS model obtained from Fig. 8*

β_i (K/Min)	T(°C)/T(K)	Ln(β_i /T^2)	1/T x 10^4
5	810/1083	-12.36	9.23
10	834/1107	-11.72	9.03
20	918/1191	-11.17	8.4

The information required for determining the activation energy is based on the KAS model shown in Table 1. The activation energy curve in terms of temperature (E_α-T) contains information obtained from Table 1 has been plotted in Fig. 8 too. The slope of line equation in the corresponding curve is -E_α /R x10^{-4}, so the amount of activation energy of the thermite reaction in the temperature range of 810 to 918°C is equivalent to 106.4 kJ/mol.

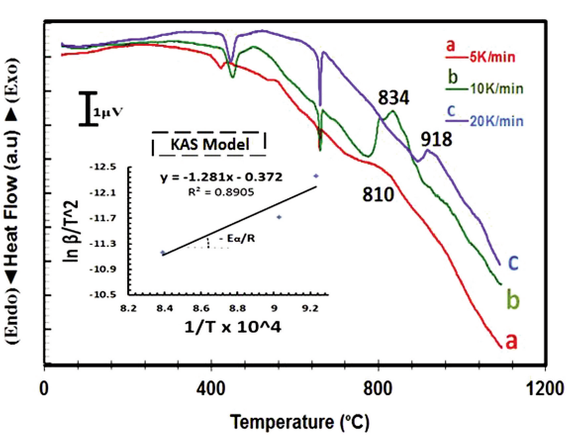

Figure 8*. DSC graphs of $FeMo_{Mix}$ sample at different heating rate of 5, 10 and 20K/min along with the activation energy diagram on the basis of KAS model*

4. Conclusions

The production of ferromolybdenum directly from aluminothermic reduction of the molybdenite (MoS_2) along with hematite in the presence of lime as a desulfurization agent by microwave-assisted combustion method is technically feasible.

Formation of intermetallic compounds like $Fe_3Mo_3C_{1-x}$ and Fe_3Mo along with slag contains noticeable solid sulfur compounds as CaS and $CaSO_4$ phases are quite observed.

DSC/TGA results showed four sequential endothermic and exothermic reactions at 420, 540, 660, and 810°C during the heating process of $FeMo_{Mix}$ specimen prepared according to $0.42MoS_2 + 1.14Al + 0.29Fe_2O_3 + 0.84CaO$ powder mixture.

Formation mechanism in this system involves evaporation of moisture and volatile matter, molybdenite roasting, production of $CaMoO_4$ and $CaSO_4$ phases as lateral compounds, aluminum melting transformation, and final SHS reaction.

The Kissinger–Akahira–Sunose (KAS) procedure, model free isoconversional kinetic analysis, was used to determine apparent activation energy in this system. The activation energy was determined as 106.4 KJ.mol^{-1} for thermite reaction in the temperature range of 810 to 918°C

Acknowledgement

Authors are highly grateful to the Ferdowsi University of Mashhad and Central Research Laboratory.

References

[1] C.K. Gupta, Extractive metallurgy of molybdenum, CRC Press, USA, 1992.

[2] M. Gasik, Technology of molybdenum ferroalloys, in: M. Gasik (editor) Handbook of Ferroalloys; Theory and Technology, Elsevier USA.2013, pp.387-396.

[3] R. H. Eric, Production of ferroalloys, in: S. Seetharaman (Editor in chief), Treatise on Process Metallurgy, industrial process Part A, Elsevier Ltd ,USA, 2014,pp. 478-530.

[4] C. J. Mahesh, Extractive metallurgy of molybdenum, in: M.Mishra (Editor), Review of extraction, processing, properties &application of reactive metals, TMS Annual Meeting, San Diego, 1999, pp.73-82.

[5] E.L. Baker, A. Daniels, G.P. Voorhis, and T. Verong, in: A. Crowson, E.S. Chen, J.A. Shields, P.R. Subramanian (Eds.), Molybdenum and Molybdenum Alloys, TMS Annual Meeting, Warrendale, PA,1998,pp.200-220

[6] A. Khoshnevisan, H. Yoozbashizadeh, J. Min. Metall. Sect. B-Metall. 48 (1) B (2012) 89 – 99

[7] R. Padilla, M.C. Ruiz, and H.Y. Sohn, Metall. Mater. Trans.B, 28B (1997) 265-274.

[8] O.k.Mehra, D.k.Bose, C.k.Gupta, , T. Indian. I. Metals. TP.698 (1973) 1-7.

[9] T.R. Mankhand, P.M. Prasad, Metall. Trans. B. 13B (1982) 276- 282.

[10] C. Lelievre. Stedman, C.A.Pickles, Plasma production of ferromolybdenum from molybdenite in the presence of sodium carbonate, in: Bergman (Editor), Ferrous and Non-ferrous Alloy Processes, Ontario, 1990, pp. 63-75.

[11] P.M.Prasad, T.M.Parkhand, Miner. Eng. 6 (1993) 857-871.

[12] P.M.Prasad, T.R. Mankhand, A.J.K. Prasad, NML. Tech. J. 39 (1997) 39-58.

[13] A.K.Suri, J.C. Sehra, and C.K. Gupta, Miner.Process.Extr.Metall. Rev. 15 (1995) 23-29.

[14] M.M.Afsahi, B.Abolpour, V.Kumar, and M. Sohrabi, Miner. Process. Extr. Metall. Rev. 34(2013)151–175.

[15] M.H.Golmakani, J.Vahdati khaki, and A.Babakhani,Mater.Chem.Phys.194 (2017) 9-16

[16] R. J. Munz, W. H. Gauvin, AlChE. Journal. 21(1975) 1132-1142.

[17] H. Nitta, K. Miura, Y. Iijima, Acta Materialia, 54 (2006) 2833–2847.

[18] M. Schoenitz, S. Umbrajkar, E. L. Dreizin, j.propul.power, 23 (2007) 673-678.

[19] B.-S. Kim, E. Kim, H.-S. Jeon, H.-I. Lee, and J.-C. Lee, Mater. Trans. 49 (2008) 2147 - 2152.

[20] B.-S. Kim, H.-I. Lee, Y.-Y. Choi,and S. Kim, Mater.Trans. 50 (2009) 2669 – 2674

[21] B-S. Kim, S-B. Kim, H-I. Lee and Y.-Y.Choi, Mater. Trans. 52 (2011) 1288 - 1293.

[22] M.Gan, X-H.Fan, X-L. Chen, C-Q. Wu, Z-Y. Ji, S-R Wang, et al., Trans. Nonferrous Met. Soc. China.26 (2016) 3015−3023.

[23] M. Sharifitabar, J. Vahdati khaki, and M. Haddad Sabzevar, Int. J. Refract. Met. Hard. Mater. 47 (2014) 93-101.

[24] A.G. Merzhanov, J. Mater.Process. Technol. 56 (1996) 222-241.

[25] L.M. Di, A. Calka, Z.L. Li, J.S. Williams, J. Appl. Phys. 78 (1995) 4118-4122.

[26] Z. Du, C. Guo, C. Li, and W. Zhang, J Phase Equilib Diff. 30 (2009) 487-501

[27] J. Houserova, J. Vrestal, and M.Sob, CALPHAD. 29 (2005) 133–139.

[28] M. Moukwa, S. Farrington and D. Youn, Thermochim. Acta, 195 (1992) 231-237.

[29] A.Yolanda, M.Alonso and J. Carlos Abanades, Industrial & Engineering Chemistry Research 53, (2014)12594-12601.

[30] Derrick Dean, Thermal Gravimetric Analysis, University of Alabama at Birmingham.https://www.uab.edu/engineering/home/images/downloads/TGA_UAB_TA_MAy_absolute_final_2014.pdf

[31] A. Chychko, L. Teng, S. Seetharaman, Steel. Res. Int. 81(2010) 784–791

[32] A. Liu , Z. Shi ,K. Xie, X. Hu, B. Gao, M. Korenko ,and Z. Wang , J. Min. Metall. Sect. B-Metall. 53 (2) B (2017) 155 – 162.

[33] B. Hu , B. Yao , J. Wang , J.-R. Zhao , F.-F. Min, and Y. Du, J. Min. Metall. Sect. B-Metall. 53 (2) B (2017) 95 – 106.

[34] J.Hammerschmidt, M. Wrobel , the Southern African Institute of Mining and Metallurgy, Sulphur and Sulphuric Acid Conference, Cape Town, south Africa, 2009, 86-100.

[35] Z. You, G. Li, Z. Peng, L. Qin, Y. Zhang, and T. Jiang, J. Min. Metall. Sect. B-Metall. 53 (2) B (2017) 115 – 122.

[36] M. Rafiei, M.H. Enayati, F. Karimzadeh, Powder. Technol. 253 (2014) 553–560.

[37] V. Leroya, D. Cancellieri, E Leoni, J-L. Ross, Thermochim. Acta. 497 (2010) 1–6.

[38] R. Ebrahimi Kahrizsangi, M.H.Abbasi, A.Saidi, Iran. J. Chem. Chem. Eng. 26, (2007), 119-123.

[39] P. Šimon, J. Therm. Anal. Calorim. 76 (2004) 123–132.

MEHANIZAM FORMIRANJA Fe-Mo PREDLEGURE ALUMINOTERMIČKOM REDUKCIJOM MoS_2-Fe_2O_3 U PRISUSTVU KREČA

M.H. Golmakani, J. Vahdati khaki*, A. Babakhani

Odsek za metalurško inženjerstvo, Tehnički fakultet, Firdusi univerzitet u Mešhedu, Mešhed, Iran

Apstrakt

U ovom radu je ispitivan mehanizam reakcije aluminotermičke redukcije MoS_2-Fe_2O_3 u prisustvu kreča koristeći metod sinteze sagorevanjem u mikrotalasnoj pećnici. Ovaj postupak se odlikuje dobijanjem feromolibdena u jednom koraku uz odvajanje sumpora u čvrstom obliku. Simultana termalna analiza (DSC/TGA) i rendgenska difrakcija tokom postupka zagrevanja $0.42MoS_2 + 1.14Al + 0.29Fe_2O_3 + 0.84CaO$ pokazale su da postoje četiri glavne sekvencijalne endotermičke i egzotermičke reakcije na 420, 540, 660 i 810°C. Najznačajnije reakcije obuhvataju isparavanje vlage i drugih isparljivih materija, prženje molibdenita, istovremeno dobijanje sporednih jedinjenja kao što su $CaMoO_4$ i $CaSO_4$, prelaz aluminijuma u topljivo stanje, kao i konačna reakcija termita. Ispitivanje kinetike postupka je sprovedeno uz pomoć klasičnog pristupa Kisindžer-Akahira-Sunoze metode (KAS). U ovom radu je određena aktivaciona energija od 106.4 ($kJ.mol^{-1}$) za reakciju termita u temperaturnom opsegu od 810 do 918°C.

Ključne reči: *Aluminotermička redukcija; Termo-analitički; Feromolibden; Kinetika; Aktivaciona energija*